Journal of Nuclear Medicine, published on April 19, 2018 as doi:10.2967/jnumed.118.210013

Comparative Study of the Novel RGD Motif-containing αvβ6 Integrin Binding Peptides SFLAP3 and SFITGv6 for Diagnostic Application in HNSCC

Saskia Roesch[1,2*], Thomas Lindner[3*], Max Sauter[3,6*], Anastasia Loktev[4], Paul Flechsig[5], Martin Müller[4], Walter Mier[3], Rolf Warta[1,2], Gerhard Dyckhoff[1], Christel Herold-Mende[1,2], Uwe Haberkorn[3,4], Annette Altmann[3,4]

*** Authors contributed equally to the work**

Affiliations:

1. Department of Otorhinolaryngology, University Hospital Heidelberg, Germany
2. Division of Experimental Neurosurgery, Department of Neurosurgery, University Hospital Heidelberg, Germany
3. Department of Nuclear Medicine, University Hospital Heidelberg, Germany
4. Clinical Cooperation Unit Nuclear Medicine, German Cancer Research Center (DKFZ), Heidelberg, Germany
5. Department of Radiology, University Hospital Heidelberg, Germany
6. Department of Clinical Pharmacology and Pharmacoepidemiology, University Hospital Heidelberg, Germany

Corresponding author:

Annette Altmann, Department of Nuclear Medicine, University Hospital Heidelberg, INF400, 69120 Heidelberg, Germany

Phone: +496221-567571; Fax: +496221-568575; E-Mail: A.Altmann@dkfz.de

First authors:

Saskia Roesch, Thomas Lindner, Max Sauter, University Hospital Heidelberg, INF400, 69120 Heidelberg, Germany

Key Words: αvβ6 integrin; novel peptide; head and neck squamous cell carcinoma; PET

Short running title: Alpha v beta 6 Integrin Binding Peptides

ABSTRACT

Alpha v beta 6 (αvβ6) integrin is overexpressed by several carcinomas and thus considered as target for diagnostic imaging and anti-cancer therapies. Recently, we presented SFITGv6 as a novel potential tracer for imaging and targeted therapy of αvβ6 integin-positive carcinomas. Here, we analyzed affinity and specificity of five native αvβ6 integrin-specific binders in comparison to SFITGv6.

Methods: Sunflower trypsin inhibitor (SFTI)-1-based peptides containing arginine-glycine-aspartic acid (RGD) motif-spanning octamers of fibronectin (SFFN1), tenascin C (SFTNC), vitronectin (SFVTN), and latency-associated peptides (LAP) 1 (SFLAP1), and 3 (SFLAP3) were synthesized and their binding potential to αvβ6 integrin-expressing head and neck squamous cell carcinoma (HNSCC) cell lines was evaluated. Subsequently, stability, affinity and specificity were assessed *in vitro* using radio-high pressure liquid chromatography, surface plasmon resonance (SPR) assay, and binding experiments including competition, kinetics, internalization, and efflux. αvβ6 integrin binding specificity was further evaluated by peptide histochemistry. Finally, *in vivo* binding properties were assessed using small-animal positron emission tomography (PET) imaging and biodistribution experiments in HNSCC-bearing mice and ^{68}Ga-DOTA-SFLAP3 was applied for diagnostic positron emission tomography/computed tomography (PET/CT) of a HNSCC patient. **Results:** Comparing the newly designed peptides significant binding (>20%) to several HNSCC cell lines (HNO97, HNO399, and HNO223) and a fast internalization of up to 60% and 70% was observed for SFLAP3 (G**RGD**LGRL) and SFITGv6 (F**RGD**LMQL). In contrast, the other peptides displayed moderate (SFLAP1: 4.1-12.1%) to marginal binding (SFFN1, SFTNC and SFVTN: <1%) and were, therefore, excluded from further analysis. Notably, SFLAP3 exhibited improved affinity for αvβ6 integrin (IC_{50}mean = 3.5 nM; K_D = 7.4). Moreover, small-animal positron emission tomography (PET) imaging and biodistribution studies of HNSCC xenograft mice revealed an increased tumor-specific accumulation 30-60 min after injection of ^{177}Lu-labeled and/or ^{68}Ga-DOTA-labeled SFLAP3. Peptide staining further

demonstrated binding specificity of SFLAP3 to HNSCC tumor cells. Finally, PET/CT scan of an HNSCC patient showed specific SFLAP3 accumulation in the primary tumor lesion (standardized uptake values (SUV)max = 5.1) and in a corresponding lymph node metastases (SUVmax = 4.1). **Conclusion:** SFLAP3 represents a promising tracer for prognostic assessment, diagnostic imaging and possibly targeted therapy of αvβ6 integrin-expressing tumors.

INTRODUCTION

Integrins comprise a large family of cellular adhesion receptors that play an important role in development, immune response, and cancer (*1-3*). Unlike most epithelial integrins, αvβ6 integrin is upregulated in many carcinomas associated with poor prognosis including lung, ovarian, pancreatic, colorectal, and cervical cancer (*4-8*). In contrast, healthy tissues show no or a rather low αvβ6 integrin expression (*9*). Therefore, it is considered as prognostic biomarker and as an important target for imaging and anti-cancer therapies (*10,11*). Using a sunflower trypsin inhibitor (SFTI)-1-based phage display library for biopanning against head and neck squamous cell carcinoma (HNSCC) cells and fractionated high pressure liquid chromatography-derived membrane proteins we identified the novel αvβ6 integrin-specific peptide SFITGv6 (*12*). Due to the molecular scaffold of SFTI-1, a 14-residue cyclic miniprotein isolated from sunflower seeds which is stabilized by a single disulfide bridge, the peptide exhibits excellent stability (*13*). SFITGv6 demonstrates high binding affinity to several αvβ6 integrin-positive tumor cells and to HNSCC xenografts. Moreover, it accumulates in tumor lesions of HNSCC and non-small cell lung carcinoma, but not in inflammatory lesions of cancer patients (*12*).

αvβ6 integrin binds the tripeptide recognition sequence arginine-glycine-aspartic acid (RGD) of several extracellular matrix proteins, including fibronectin, vitronectin, tenascin C, and latency-associated peptides (LAP) 1 and 3 that participate in carcinogenesis by promoting cell migration and invasion of cancer cells (*14,15*). Particularly, αvβ6 integrin-mediated TGF-β activation plays an important role in epithelial to mesenchymal transition and thereby promotes tumor growth and metastasis (*16*). Non-covalently associated with the N-terminus of TGF-β1 and TGF-β3 LAP prevents TGF-β from binding to TGF-β receptors. Binding of LAP1 or LAP3 to αvβ6 integrin induces the dissociation of the complex followed by TGF-β activation (*17,18*). Considering both, the requirement of additional tumor-specific peptides targeting epithelial tumors and the high stability of the SFTI-1 scaffold (*13*), we designed further RGD sequence-containing SFTI-1 derivates (SFFN1, SFTNC, SFVTC, SFLAP1, and SFLAP3) and compared

αvβ6 integrin-specific binding properties with those of SFITGv6. Thus, we discovered SFLAP3; a peptide that demonstrates high αvβ6 integrin affinity and specificity for several αvβ6 integrin-expressing tumor cells. Moreover, SFLAP3 displays an increased accumulation in HNSCC xenografts and patient tumors.

MATERIALS AND METHODS

Cell Lines, Tumor Material, and Ethical Approval

The HNSCC-derived cell lines HNO97, HNO199, HNO210, HNO223, and HNO399 (*19*) were cultured in RPMI 1640 medium supplemented with 10% FCS at 37°C and 5% CO_2 and were negative for *Mycoplasma* contamination. Uniqueness was assessed by the German Collection of Microorganisms and Cell Culture. Patient-derived tumor tissues obtained intraoperatively were snap-frozen and stored at -80°C. Written informed consent was obtained from all patients according to the research proposals approved by the Institutional Review Board at the Medical Faculty of the University of Heidelberg.

In Vitro Binding Experiments

For assessment of the peptide binding capacity *in vitro*, 2.5-4x10^5 cells were seeded into 6-well plates and cultivated for 48 h. The cells were exposed to ^{125}I-labeled peptides resuspended in 1 mL serum-free medium for 10 or 60 min either with or without different concentrations of unlabeled peptide (10^{-5}-10^{-10} M). Unbound peptide was washed off (3 x phosphate-buffered saline) and finally, cells were harvested using 0.3 M NaOH. To evaluate kinetic properties, cells were exposed to ^{177}Lu-DOTA-labeled peptides for 10, 30, 60, 120, 360, and 480 min, respectively, and lysed as described. Efflux was assessed by incubating the cells with ^{177}Lu-DOTA-labeled peptides for 60 min. Next, radioactive peptide-containing medium was replaced and the cells were incubated for another 10, 30, 60, 120, and 240 min and finally lysed as described. To assess peptide internalization, cells were exposed to ^{177}Lu-DOTA-labeled peptides for 10, 30, 60, 120, and 240 min at 37°C. Surface bound peptides were removed by 10 min incubation with 1 M glycine-HCl solution (pH 2.2). Cells were rinsed with phosphate-buffered saline and lysed as described. Radioactivity was determined in a γ-counter (LB951G, Berthold Technologies) and calculated as percentage of injected dose radioactivity (MBq) per 10^6 cells (% ID/10^6 cells).

Surface Plasmon Resonance (SPR) Assay

Binding affinity was assessed via BiaCore X100 (GE Healthcare) as described in detail previously (*12*). Briefly, to prevent integrin heterodimer-denaturation during immobilization αvβ6 (1, 2, 3, and 4 µg/mL) and αvβ3 integrin (15, 30, 35 and 40 µg/mL) were used as analytes. SFLAP3 was dissolved in HBS-EP running buffer and immobilized (loading level: 12 response units) on the C1 sensor chip (both GE Healthcare) using a manual amine coupling protocol. Next, binding affinity of αvβ6 and αvβ3 integrin, respectively, dissolved in HBS-EP running buffer (1-50 µg/mL) to SFLAP3 was measured (flow rate: 30 µL/min). The dissociation constant (K_D) was determined by a 1:1 Langmuir model fit of the SPR sensograms.

Animal Experiments

Animal experiments were conducted in compliance with the German animal protection laws. For *in vivo* small-animal positron emission tomography (PET) imaging and organ distribution studies eight-week old Balb/c nude mice (Charles River Laboratories) were inoculated subcutaneously at the right shoulder with a total of $5x10^6$ tumor cells in MatriGel (BD Bioscience).

Xenografts were grown until a 10-15 mm tumor diameter. Mice were anesthetized using isofluorane inhalation and a 100 µL phosphate-buffered saline solution containing ^{68}Ga-DOTA-SFLAP3 (HNO97: 37.9 MBq; HNO399: 26 MBq; HNO223: 27 MBq) or ^{68}Ga-DOTA-SFITGv6 (HNO97: 30 MBq; HNO399: 34 MBq; HNO223: 34 MBq) was injected into the tail vein. 3-dimensional PET images were captured (Siemens Inveon PET scanner) as described (*12*). To assess the biodistribution, 100 µL of a 20 nM ^{177}Lu-DOTA-SFLAP3 or ^{177}Lu-DOTA-SFITGv6 solution (1 MBq) was administered as an intravenous bolus injection into the tail vein. For each point of time (30-360 min) we sacrificed three animals, collected peripheral blood and the respective organs, weighted the tissues, and measured the radioactivity using a γ-counter. Values were expressed as percentage of the injected dose radioactivity (MBq) per gram tissue (% ID/g).

Peptide Staining

Histochemical stainings were performed using biotinylated PEG(12)-labeled peptides on acetone-fixed cryosections (5 µm) derived from snap-frozen HNSCC tissues as described previously (*12*). Briefly, to prevent background staining HNSCC cryosections were pre-incubated with the Avidin/Biotin Blocking Kit (SP-2001, Vector Laboratories) and subsequently 10^{-5} M peptide diluted in Antibody Diluent (DAKO) was applied at 4°C, overnight. Detection of bound peptide was assessed by using the Vectastain Elite ABC Kit (PK-6100, Vector Laboratories) according to manufacturer´s instructions. Peptide-binding specificity was ensured by using a peptide containing a scrambled (GRD) sequence and by incubation without peptide. Due to instability of the peptide binding, stainings were assessed on the same day as described before.

PET/CT Scan of HNSCC Tumor Patient

A non-contrast-enhanced PET/CT scan was performed 60 and 180 min after intravenous injection of the ^{68}Ga-DOTA-labeled peptide using a SIEMENS-BIOGRAPH mCt Flow™ PET/CT-Scanner (Siemens Medical Solution) and the following parameters: slice thickness of 5 mm, increment of 3-4 mm, soft-tissue reconstruction kernel, Care dose. Immediately after CT scanning, a whole body PET was acquired in 3-D (matrix 200x200) in FlowMotion with 0.7 cm/min. The emission data were corrected for randoms, scatter, and decay. Reconstruction was conducted with an ordered subset expectation maximisation algorithm with 2 iterations/21 subsets and Gauss-filtered to a transaxial resolution of 5 mm at full-width half-maximum. Attenuation correction was performed using the low-dose non-enhanced CT data. The quantitative assessment of tracer accumulation was done using a region of interest technique and using standardized uptake values (SUV).

RESULTS

Binding of SFTI-1 Derivates to αvβ6 Integrin-Expressing HNSCC Cell Lines

RGD motif-containing octamers of the natural αvβ6 integrin-ligands fibronectin, tenascin C, vitronectin, LAP1, and LAP3 (Supplemental Table 1) were grafted between Thr4 and Cys11 into the binding loop of the SFTI-1 scaffold. First, the binding properties of ^{125}I-labeled SFFN1, SFTNC, SFVTN, SFLAP1 SFLAP3, and SFITGv6 were compared using five HNSCC cell lines differing in their αvβ6 integrin-expression as assessed by flow cytometry (Supplemental Fig. 1). As shown in figure 1A ^{125}I-SFLAP3 displayed the highest binding capacity to all tested HNSCC cell lines (HNO97 = 24.7%, HNO399 = 10.1%, HNO199 = 19.7%, HNO223 = 17.6%, HNO210 = 10.6%) which was even higher as compared to ^{125}I-SFITGv6 (HNO97 = 21.8%, HNO399 = 9.8%, HNO199 = 16.8%, HNO223 = 13.5%, HNO210 = 10.5%). In contrast, only moderate binding capacity was detected for SFLAP1 (4.1-12.1%) and almost none (<1%) for SFFN1, SFTNC and SFVTN (Fig. 1A). In summary, SFLAP3 and SFITGv6 demonstrated the highest binding capacity and, thus, were further investigated comparatively.

SFLAP3 Exhibits Improved Affinity for αvβ6 Integrin and Excellent Serum Stability

To assess the specificity of the peptide binding competition experiments were performed. In all HNSCC cell lines, binding of ^{125}I-SFLAP3 and ^{125}I-SFITGv6 could almost be completely competed by adding 10^{-6} M unlabeled counterparts as competitor (Figs. 1B and 1C). However, SFLAP3 exhibited higher affinity (IC_{50}mean = 3.5 nM) when compared to SFITGv6 (IC_{50}mean = 14.11 nM). Concordantly, the SPR assay revealed higher affinity of SFLAP3 for αvβ6 integrin (K_D = 7.4 nM) (Fig. 1D) when compared to SFITGv6 (K_D = 14.8 nM) (*12*). In contrast, we observed a 10-fold lower affinity of SFLAP3 to αvβ3 integrin (K_D = 167 nM) (Supplemental Fig. 2A), further ensuring αvβ6 integrin-specificity of SFLAP3. Additionally, SFLAP3 demonstrated high proteolytic stability with no degradation over 24 hrs (Supplemental Fig. 2B), demonstrating the suitability of SFLAP3 for *in vivo* applications.

Comparative Evaluation of Kinetic, Internalization, and Efflux

Considering time-dependent deionization of iodine 125 the determination of kinetic, internalization, and efflux was performed using ^{177}Lu-DOTA-labeled peptides. Kinetic experiments revealed a continuous increase in peptide uptake over the whole period of measurement for both peptides. Yet, ^{177}Lu-DOTA-SFLAP3 exhibited a lower maximum binding capacity (HNO97 = 18.5%, HNO223 = 9.66%, HNO399 = 4.31%) (Supplemental Fig. 3A) when compared to ^{177}Lu-DOTA-SFITGv6 (HNO97 = 22.15%, HNO223 = 14.45%, HNO399 = 5.85%), (Supplemental Fig. 3B). Accordingly, within 60 min after exposure to HNO97 we measured an increase of ^{177}Lu-DOTA-SFITGv6 binding of up to 16.85% and a fast internalization of up to 70% of the total bound peptide (Fig. 2B), but up to 11.14% binding and 60% internalization of ^{177}Lu-DOTA-SFLAP3 (Fig. 2A). For both peptides similar trends regarding time-dependent increase of peptide-binding and internalization were observed after exposure to HNO399 (Supplemental Figs. 4A and 4B) and HNO223 (Supplemental Figs. 4C and 4D), although the amount of internalized peptide slightly decreased (>45%). Concordantly, an efflux of more than 50% of the originally accumulated SFLAP3 and SFITGv6 within 120 min after the termination of the uptake was measured (Figs. 3A and 3B). Notably, for ^{177}Lu-DOTA-SFLAP3 we observed a moderate renewed increase of binding/internalization after 240 min (Fig. 3A), which may indicate a peptide re-uptake from the culture medium.

***In Vivo* Targeting Properties of SFLAP3 and SFITGv6**

To compare the *in vivo* targeting properties of the peptides small-animal PET imaging of HNO97-, HNO399-, and HNO223-xenografts were performed using ^{68}Ga-DOTA-labeled SFLAP3 and SFITGv6 as radiotracer. In HNO97 tumor lesions a fast and continuous accumulation of ^{68}Ga-DOTA-SFLAP3 (SUV mean = 0.63) (Fig. 4A; Supplemental Fig. 5A) and ^{68}Ga-DOTA-SFITGv6 (SUVmean = 0.68) (Supplemental Figs. 5B and 5C) was measured within 60 min after injection which stayed for at least 140 min (Supplemental Figs. 5D and 5E). Non-specific peptide activity cleared quickly from the blood resulting in images with excellent tumor-

to-background ratios. Accordingly, the biodistribution of ^{177}LuDOTA-SFLAP3 in tumor lesions and individual organs of HNO97-xenografts revealed maximal peptide accumulation in the tumors after 60 min (9.1±1.2% ID/g), followed by a decrease to 5.80±1.44% ID/g 360 min post injection (Fig. 4B). In contrast, the maximal uptake of ^{177}Lu-DOTA-SFITGv6 in HNO97 tumors (6.73±1.00% ID/g) was measured already 30 min post injection and decreased to 2.43±0.51 % ID/g after 360 min (Supplemental Fig. 5F). Small-animal PET imaging of HNO399- (Fig. 4C; Supplemental Fig. 6B) and HNO223-xenografts (Supplemental Figs. 7A and 7B) revealed less accumulation of ^{68}Ga-DOTA-SFLAP3 (HNO399: SUVmean = 0.44; HNO223: SUVmean = 0.32) (Supplemental Figs. 6A and 7C) and of ^{68}Ga-DOTA-SFITGv6 (HNO399: SUVmean = 0.33; HNO223: SUVmean = 0.23) (Supplemental Figs. 6C and 7D). Accordingly, we measured a maximal ^{177}Lu-DOTA-SFLAP3 accumulation of 3.6% ID/g (Fig. 4D) and 3.4% ID/g (Supplemental Fig. 7E) in tumor lesions of HNO399- and HNO233-xenografts, respectively, 60 min post injection followed by a decrease to almost 2% 360 min after injection. Less than 1% ID/g was detected in the blood and most tissues of xenograft mice 120 min after injection of both peptides accounting for tumor-to-tissue ratios predominantly above one (Supplemental Tables 2A-D). However, in the kidneys we observed constantly high SFLAP3 retention (8% to 14% ID/g) which was indeed clearly reduced in comparison to SFITGv6 (Supplemental Fig. 5F).

SFITGv6 Demonstrates Better Binding Properties *in Situ*

In analogy to the previous experiments (*12*), we compared the binding-specificity of the peptides to sections of HNO97 xenografts and patient-derived HNO399 and HNO210 tumors by peptide histochemical staining using biotin-labeled SFLAP3 and SFITGv6. Albeit SFLAP3 showed a slightly fainter staining both peptides revealed tumor cell-specific binding, whereas lower peptide binding was observed at the stromal compartments (Fig. 5). In contrast, no binding of the GRD sequence containing peptide was observed further corroborating the specificity of the SFLAP3 peptide.

SFLAP3 Accumulates in HNSCC Lesion and Lymph Node Metastasis

Finally, we investigated the therapeutic and/or diagnostic suitability of SFLAP3 exemplarily in a 79 year old, male carcinoma patient presented with lymph node swelling in the right cervical area assuming the diagnosis cancer of unknown primary. In order to clarify the diagnosis 322 MBq 68Ga-DOTA-labled SFLAP3 was administered followed by a PET/CT scan. After 60 minutes we observed a tumor specific accumulation of SFLAP3 at the primary tumor lesion (right site of aryepiglottic folds) (Fig. 6) with a median SUVmax of 5.1 and at the right cervical areal (SUVmax = 4.1) (Supplemental Table 3). The histopathological examination of the surgically resected respective tissues proved a squamous cell carcinoma and corresponding lymph node metastases in Level II/III at the respective localizations. The correlation of PET-findings and histopathology revealed the primary tumor lesion as connective tissue with infiltrates of a moderately differentiated squamous cell carcinoma with infiltration of subepithelial connective tissue (C). The tumor lesion at the right cervical areal was classified as cyst wall and content with infiltrates of an epithelial neoplasia with solid growth pattern in histopathological analysis (B). Moderate tracer accumulation was also seen in a lymph node in the right cervical area (SUVmax = 2.2), which was histopathologically classified as lymph node infiltrated by epithelial tumor cells and neoplasia with solid growth pattern (D).

DISCUSSION

SFTI-1 has already been proven to be a suitable scaffold for the development of extremely stable peptides targeting tumor-associated receptors including the αvβ6 integrin-specific peptide SFITGv6 (*12, 20*). αvβ6 integrin has been shown to be expressed in up to 99.9% of HNSCC (*9,14*) as well as lung (*4*) colon (*7*), breast (*21*) and pancreas carcinoma (*6*) and is often associated with poor prognosis (*9*). Thus, αvβ6 integrin represents an important target for imaging and therapy for a variety of epithelial malignancies (*22-25*). In order to design novel target-specific peptides we introduced the RGD-containing octamer of natural αvβ6 integrin ligands resembling the RGDLXXL sequence into the SFTI-1 scaffold and evaluated specificity and affinity of the novel peptides in comparison to SFITGv6.

Comparing the binding properties of these SFTI-1 derivates we identified the αvβ6 integrin-specific peptide SFLAP3 containing the amino acid sequence GRGDLGRL. Comparative analysis of SFLAP3 and SFITGv6 revealed improved binding (>20%) of the novel peptide to several HNSCC cell lines corresponding to their αvβ6 integrin-expression profile. Considering the importance of the RGDLXXL motif – in particular the DLXXL sequence – for αvβ6 integrin binding affinity and specificity (*26-28*) it is not surprising that SFLAP3 provides significant binding properties. In contrast, for SFLAP1, SFFN1, SFVTN, and SFTNC partially or completely lacking the LXXL motif we observed less or even almost no binding. Although being physiologically involved in αvβ6 integrin-dependent promotion of migration, invasion, and signal transduction pathways (*14*), the RGD motif-containing sequences of LAP1, fibronectin, vitronectin, and tenascin C incorporated into the SFTI-1 scaffold might not allow for αvβ6 integrin affinity and specificity *in vitro*.

As expected from stability analysis of the naturally occurring SFTI-1(*13*) and the SFTI-1 derivates DLL4 (*20*) and SFITGv6 (*12*) SFLAP3 also demonstrated marked stability in human serum over 24 hrs. Additionally, an improved affinity of SFLAP3 (K_D = 7.4 nM) for αvβ6 integrin when compared to SFITGv6 was measured. Subsequent investigation of ^{177}Lu-DOTA-labeled

SFLAP3 and SFITGv6 regarding kinetics, internalization, and efflux revealed a continuously increase of SFLAP3 binding (up to 18.5% within 240 min) and a fast internalization (>60%) followed by a decrease (<50%). Correspondingly, we observed >50% efflux and almost 50% retention of the originally accumulated peptide over 120 min justifying further *in vivo* evaluation. These experiments also demonstrated a consistent up to 5.7% higher binding of ^{177}Lu-DOTA-labeled SFITGv6 when compared to that of SFLAP3. Thinkable is, that chemical properties of the SFLAP3 and SFITGv6 amino acids composition differently influence the binding capacity of DOTA-labeled peptides.

Based on excellent tumor-to-background ratios we were able to selectively image HNSCC xenografts in small-animal PET scans 60 to140 min after the administration of ^{68}Ga-DOTA-labeled SFLAP3 and SFITGv6. Unbound and unspecific bound peptide rapidly cleared from the blood and the surrounding tissues, except for the kidneys. As expected from the αvβ6 integrin expression profile of HNSCC cell lines we detected a rather low, but clearly visible accumulation of both ^{68}Ga-DOTA-SFLAP3 (SUVmean = 0.63) and ^{68}Ga-DOTA-SFITGv6 (SUVmean = 0.68) in HNO97 xenografts. In contrast, HNO399 and HNO223 xenograft tumors showed a lower uptake of the ^{68}Ga-DOTA-labeled peptides, but a generally higher affinity of ^{68}Ga-DOTA-SFLAP3 (SUVmean = 0.44; SUV = 0.32) when compared to ^{68}Ga-DOTA-SFITGv6 (SUVmean = 0.32; SUVmean = 0.23). The biodistribution of ^{177}-DOTA-labeled peptides in HNSCC xenograft mice confirmed the improved affinity of SFLAP3 for αvβ6 integrin-expressing tumors. In HNO97 tumors we found marked accumulation of SFLAP3 (up to 9.10% ID/g) and SFITGv6 (6.76% ID/g) compared to healthy tissues even after 240 and 360 minutes. In contrast, less than 4% ID/g of SFLAP3 was measured for HNO399 and HNO223 emphasizing the importance of pronounced target expression for the selective *in vivo* tumor imaging/targeting. As expected from previous biodistribution analysis of αvβ6 integrin binding peptides in HNO97 (*12*) and BxPC-3 xenografts (*11*) remarkable but slightly decreasing accumulation of ^{177}Lu-DOTA-SFLAP3 was noticed in the kidneys of HNSCC xenografts. Although the renal retention of

SFLAP3 is clearly reduced when compared to that of SFITGv6 improvement of the pharmacokinetic properties of the peptide would be recommendable.

Even though peptide-based histochemical stainings revealed a moderate but tumor cell-specific binding of SFLAP3 HNO97 xenograft and patient-derived HNSCC tumor cyrosections the ^{68}Ga-DOTA-labeled peptide was successfully used as a radiotracer for PET/CT imaging of a patient suffering from a carcinoma of unknown primary leading to the discovery of a histologically proven HNSCC and a corresponding lymph node metastasis. In line with the small-animal PET imaging results of HNSCC xenografts the SUV values in the patient persisted from 60 min (SUVmax = 5.1) to 180 min (SUVmax = 4.6) after injection demonstrating the diagnostic suitability of the peptide.

In analogy to ^{68}Ga-DOTA-SFITGv6-PET/CT of a HNSCC and a non-small cell lung carcinoma patient (*12*) the ^{68}Ga-DOTA-SFLAP3-PET/CT revealed peptide accumulation in the kidneys and gastrointestinal secretion followed by an intraluminal transport to the terminal ileum and the cecum. Thus, considering SFLAP3 for imaging of αvβ6 integrin-positive carcinomas occurring below the diaphragm administration of laxatives (reducing intra-bowel activity and avoid a high background) as well as the improvement of the pharmacokinetic properties of the peptide is required.

CONCLUSION

In conclusion, we identified the αvβ6 integrin binding peptide SFLAP3 providing improved affinity and excellent binding properties for αvβ6 integrin-expressing HNSCC tumors *in vitro* and *in vivo*. Thus, SFLAP3 represents a promising tracer for both, diagnostic imaging and also targeted therapy of αvβ6 integrin-expressing tumors.

FUNDING

This project was supported by the Deutsche Forschungsgemeinschaft (DFG) (HA 2901/12-1)

DISCLOSURE STATEMENT

No potential conflicts of interest were disclosed.

ACKNOWLEDGEMENTS

We thank Vanessa Kohl and Marlene Tesch for technical assistance as well as Ursula Schierbaum and Karin Leotta for performing animal experiments. We also thank Dr. Esther Herpel (Tissue Bank, National Center for Tumor Diseases (NCT) Heidelberg, Germany) for the histopathological examination of tumor tissues and Dr. Carmen Rapp for proofreading.

REFERENCES

1. Zhang Y, Wang H. Integrin signalling and function in immune cells. *Immunology*. 2012;135:268-275.

2. Seguin L, Desgrosellier JS, Weis SM, Cheresh DA. Integrins and cancer: regulators of cancer stemness, metastasis, and drug resistance. *Trends Cell Biol*. 2015;25:234-240.

3. Desgrosellier JS, Cheresh DA. Integrins in cancer: biological implications and therapeutic opportunities. *Nat Rev Cancer*. 2010;10:9-22.

4. Elayadi AN, Samli KN, Prudkin L, et al. A peptide selected by biopanning identifies the integrin αvβ6 as prognostic biomarker for nonsmall cell lung cancer. *Cancer Res.* 2007;67:5889-5895.

5. Ahmed N, Riley C, Rice GE, Quinn MA, Baker MS. $\alpha_v\beta_6$ integrin-A marker for the malignant potential of epithelial ovarian cancer. *J Histochem Cytochem*. 2002;50:1371-1379.

6. Sipos B, Hahn D, Carceller A, et al. Immunohistochemical screening for β6-integrin subunit expression in adenocarcinomas using a novel monoclonal antibody reveals strong up-regulation in pancreatic ductal adenocarcinomas *in vivo* and *in vitro*. *Histopathology*. 2004;45:226-236.

7. Bates RC, Bellovin DI, Brown C, et al. Transcriptional activation of integrin β6 during the epithelial-mesenchymal transition defines a novel prognostic indicator of aggressive colon carcinoma. *J Clin Invest*. 2005;115:339–347.

8. Hazelbag S, Kenter GG, Gorter A, et al. Overexpression of the alpha v beta 6 integrin in cervical squamous cell carcinoma is a prognostic factor for decreased survival. *J Pathol.* 2007;212:316–324.

9. Bandyopadhyay A, Raghavan S. Defining the role of integrin alphavbeta6 in cancer. *Curr Drug Targets.* 2009;10:645–652.

10. Hackel BJ, Kimura RH, Miao Z, et al. 18F-fluorobenzoate-labeled cystine knot peptides for PET imaging of integrin αvβ6. *J Nucl Med*. 2013;54:1101-1105.

11. Hausner SH, Abbey CK, Bold RJ, et al. Targeted in vivo imaging of integrin avb6 with an improved radiotracer and its relevance in a pancreatic tumor model. *Cancer Res.* 2009;69:5843-5850.

12. Altmann A, Sauter M, Roesch S, et al. Identification of a novel ITGαvβ6-binding peptide using protein separation and phage display. *Clin Cancer Res*. 2017;23:4170-4180.

13. Boy RG, Mier W, Nothelfer EM, et al. Sunflower trypsin inhibitor 1 derivatives as molecular scaffolds for the development of novel peptidic radiopharmaceuticals. *Mol Imaging Biol.* 2010;12:377-385.

14. Thomas GJ, Nyström ML, Marshall JF. Alphavbeta6 integrin in wound healing and cancer of the oral cavity. *J Oral Pathol Med*. 2006;35:1-10.

15. Annes JP, Rifkin DB, Munger JS. The integrin alphaVbeta6 binds and activates latent TGFbeta3. *FEBS Lett*. 2002;511:65-68.

16. Zavadil J, Böttinger EP. TGF-beta and epithelial-to-mesenchymal transitions. *Oncogene*. 2005;24:5764-5774.

17. Annes JP, Chen Y, Munger JS, Rifkin DB. Integrin αVβ6-mediated activation of latent TGF-β requires the latent TGF-β binding protein-1. *J Cell Biol*. 2004;165:723-734.

18. Wipff P-J, Hinz B. Integrins and the activation of latent transforming growth factor beta1 - an intimate relationship. *Eur J Cell Biol*. 2008;87:601-615.

19. Ninck S, Reisser C, Dyckhoff G, Helmke B, Bauer H, Herold-Mende C. Expression profiles of angiogenic growth factors in squamous cell carcinomas of the head and neck. *Int J Cancer*. 2003;106:34-44.

20. Zoller F, Markert A, Barthe P, et al. Combination of phage display and molecular grafting generates highly specific tumor-targeting miniproteins. *Angew Chem Int Ed Engl.* 2012;51:13136-13139.

21. Arihiro K, Kaneko M, Fujii S, Inai K, Yokosaki Y. Significance of alpha 9 beta 1 and alpha v beta 6 integrin expression in breast carcinoma. *Breast Cancer.* 2000;7:19-26.

22. Saha A, Ellison D, Thomas GJ, Vallath S, Mather SJ, Hart IR, et al. High-resolution in vivo imaging of breast cancer by targeting the pro-invasive integrin alphavbeta6. *J Pathol.* 2010;222:52–63.

23. Hausner SH, Bauer N, Hu LY, Knight LM, Sutcliffe JL. The effect of bi-terminal PEGylation of an integrin $\alpha v\beta_6$-targeted 18F peptide on pharmacokinetics and tumor uptake. *J Nucl Med*. 2015;56:784-790.

24. Zhu X, Li J, Hong Y, et al. 99mTc-labeled cystine knot peptide targeting integrin αvβ6 for tumor SPECT imaging. *Mol Pharm.* 2014;11:1208-1217.

25. Kimura RH, Teed R, Hackel BJ, et al. Pharmacokinetically stabilized cystine knot peptides that bind alpha-v-beta-6 integrin with single-digit nanomolar affinities for detection of pancreatic cancer. *Clin Cancer Res.* 2012;18:839–849.

26. Kraft S, Diefenbach B, Mehta R, Jonczyk A, Luckenbach GA, Goodman SL. Definition of an unexpected ligand recognition motif for alphav beta6 integrin. *J Biol Chem.* 1999;274:1979–85.

27. DiCara D, Rapisarda C, Sutcliffe JL, et al. Structure-function analysis of Arg-Gly-Asp helix motifs in alpha v beta 6 integrin ligands. *J Biol Chem.* 2007;282:9657-9665.

28. Nothelfer E-M, Zitzmann-Kolbe S, Garcia-Boy R, et al. Identification and characterization of a peptide with affinity to head and neck cancer. *J Nucl Med*. 2009;50:426-434.

FIGURE LEGENDS

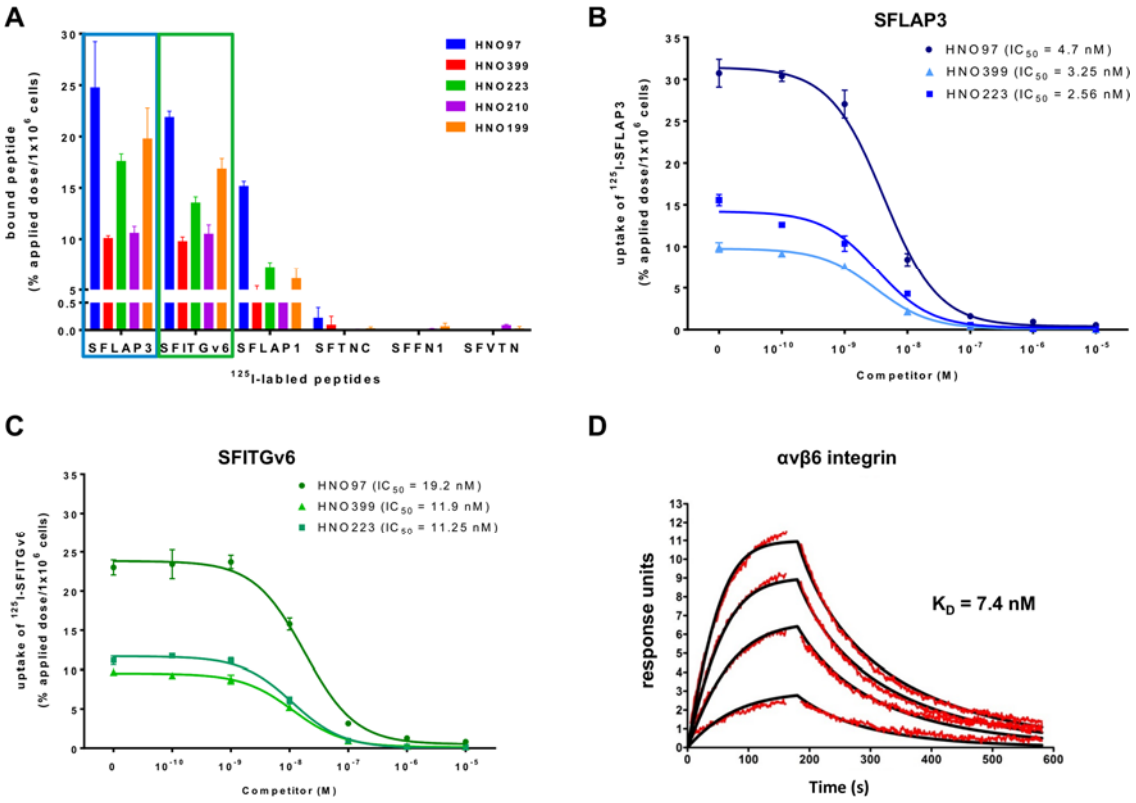

FIGURE 1: (A) Binding of ^{125}I-labeled SFLAP3, SFITGv6, SFLAP1, SFTNC, SFFN1, and SFVTN to different HNSCC cells after exposure to the peptides for 60 min. Bars represent the percentage of total bound peptide per applied dose/10^6 cells (HNO97, HNO399, HNO223, HNO210, and HNO199). Increasing concentrations (10^{-5}-10^{-10} M) of the respective unlabeled peptide was used to compete for the binding of ^{125}I-labeled SFLAP (B) and SFITGv6 (C) to HNSCC cell lines HNO97, HNO399, and HNO223 (% applied dose/10^6 cells). Data represent mean values and standard deviation of triplicate measurements from representative experiment. (D) Affinity of αvβ6 integrin (applied concentrations: 1, 2, 3 and 4 µg/mL) for immobilized SFLAP3 (loading level: 12 response units) was measured by SPR assay (n = 3) with a flow rate of 30 mL/min. The SPR-sensograms were evaluated with the BiaCore evaluation software (black curves) and correspond to the experimentally fitted red curves. K_D values were determined by a 1:1 langmuir model fit of the SPR-sensograms.

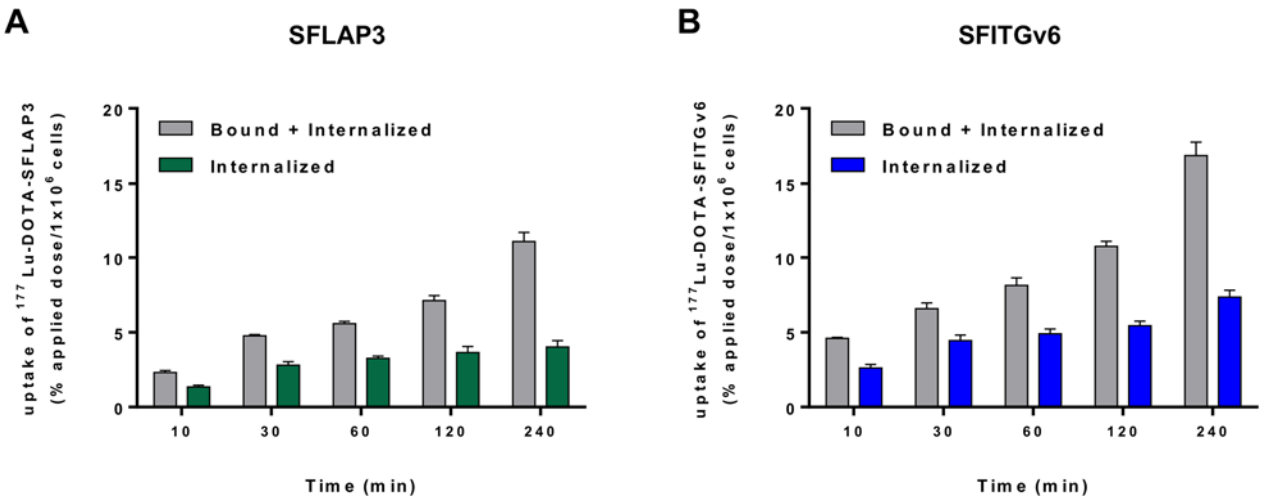

FIGURE 2: Uptake (grey bars) and internalization (colored bars) of ^{177}Lu-DOTA-labeled SFLAP3 (A) and SFITGv6 (B) in HNO97 cells. After incubation for 10, 30, 60, 120, and 240 min, respectively, the radioactivity in the lysates was determined and calculated as % applied dose/10^6 cells. Data represent mean values and standard deviation of triplicate measurements from representative experiment.

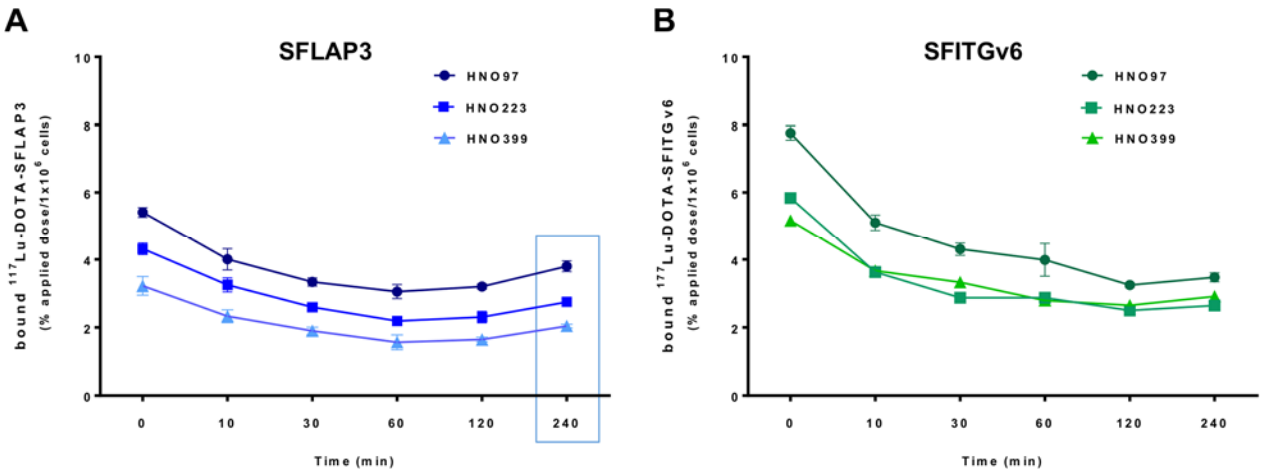

FIGURE 3: Time-dependent efflux of SFLAP3 (A) and SFITGv6 (B) from HNSCC cell lines. HNO97, HNO399, and HNO223 cells were exposed to ^{177}Lu-DOTA-labeled peptides for 60 min. After replacement of the culture medium the radioactivity in cell lysates was measured immediately and after 10, 30, 60, 120, 240 min and calculated as % applied dose / 10^6 cells. Data represent mean values and standard deviation of triplicate measurements from representative experiment.

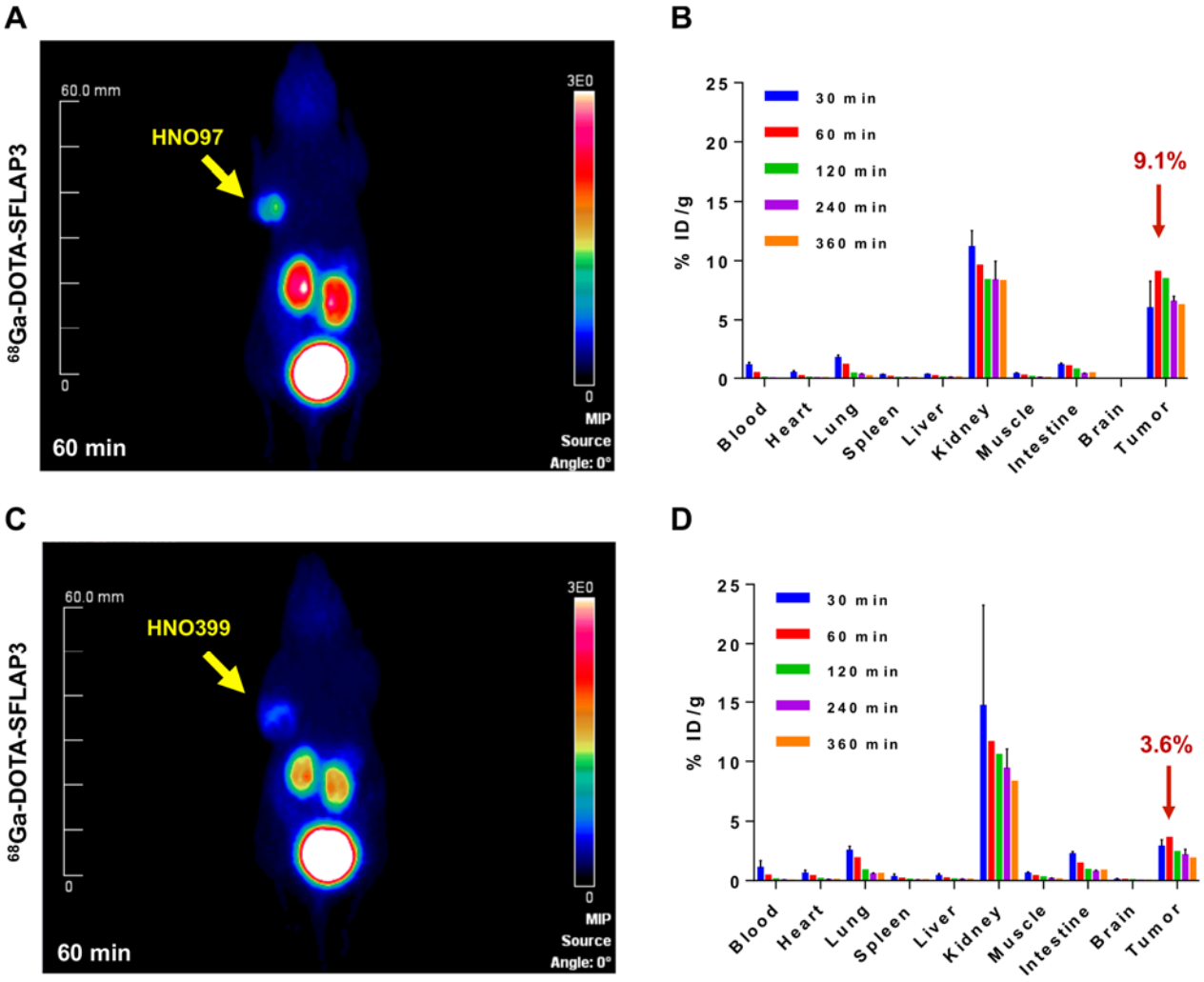

FIGURE 4: Small-animal PET imaging of mice bearing (A) HNO97 and (C) HNO399 xenografts 60 min after injection of ^{68}Ga-DOTA-SFLAP3. Biodistribution of ^{177}LU-DOTA-SFLAP3 in the tumor and organs of (B) HNO97 and (D) HNO399 tumor-bearing mice was measured 30, 60, 120, 240, and 360 min after injection and calculated as % ID/g. Data represent mean of three per time point and standard deviation.

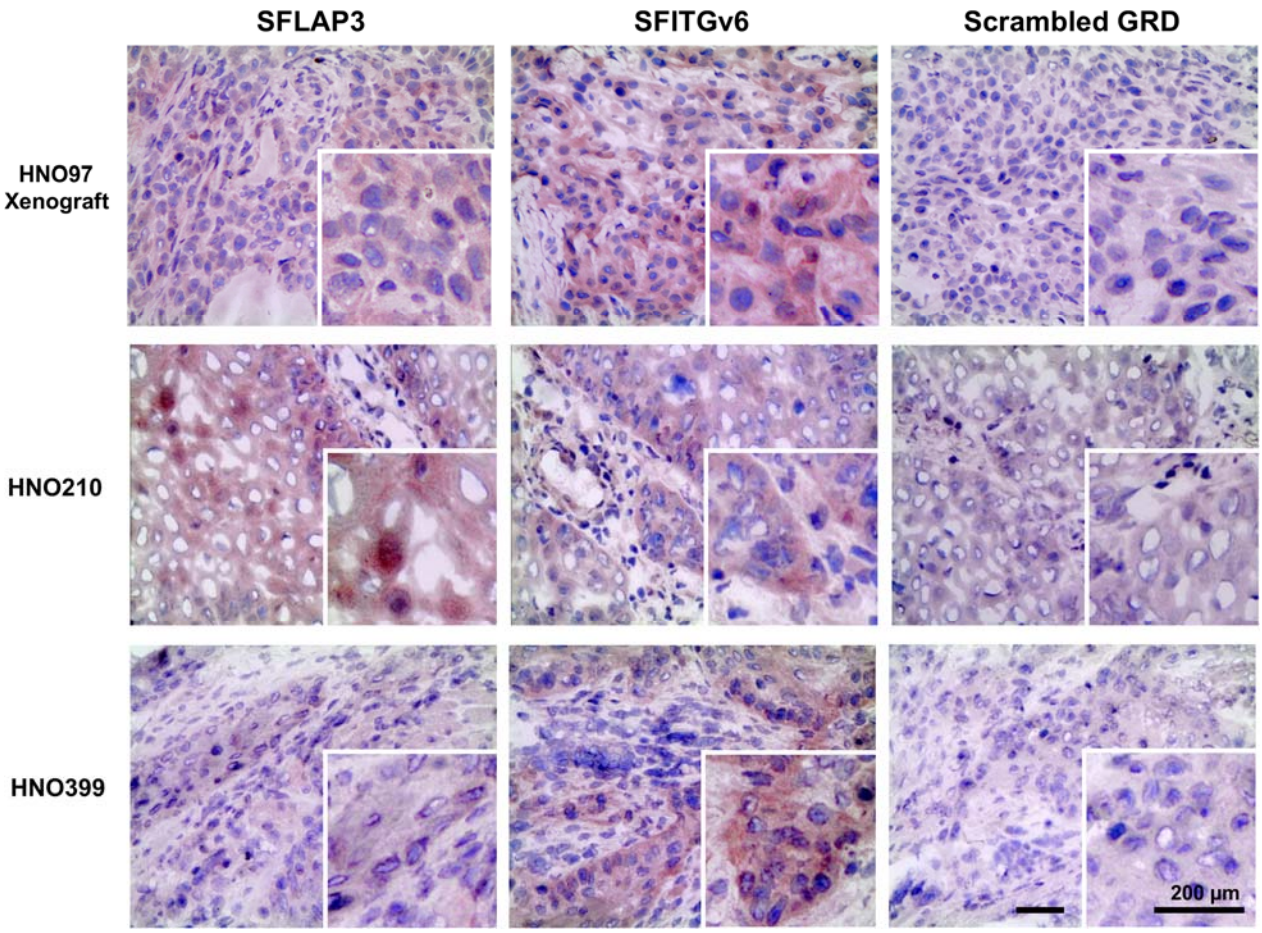

FIGURE 5: Histochemical peptide staining of HNSCC cyrosections of HNO97 xenografts and of patient-derived HNO399 and HNO210 tumor sections performed with 10^{-5} M biotinylated PEG(12)-labeled SFLAP3 and SFITGv6. As control the scrambled SFLAP3 derivate containing GRD was applied. Scale bar = 50µm.

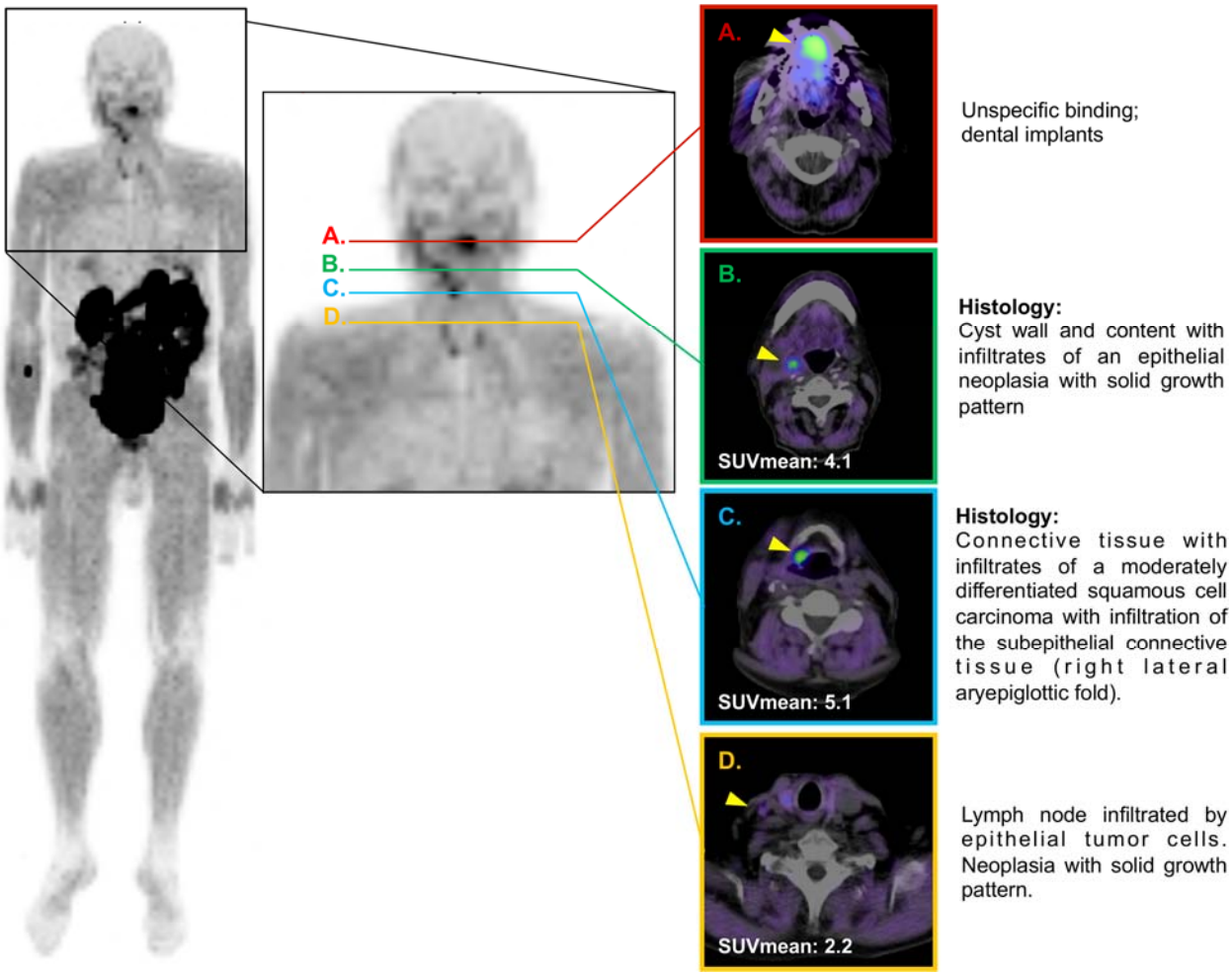

FIGURE 6: PET/CT scans of a HNSCC tumor patient after application of 322 MBq ^{68}Ga-DOTA-SFLAP3. (A-D) Transaxial slices of the PET/CT fusion images. Yellow arrows indicate peptide accumulation.

SUPPLEMENTAL METHODS

Flow Cytometry

The αvβ6 integrin expression of HNSCC cell lines was analyzed by flow cytometry (LSR II, BD Biosciences) using a primary rat monoclonal antibody against human αvβ6 integrin (Abcam, ab97588, 3 µg/mL, 1 hour, 4°C) followed by incubation with the anti-rat Alexa Fluor 488-conjugated secondary antibody (Abcam, ab150153, 1 µg/mL, 30 min, 37°C). Antigen specificity was ensured by an isotype-matched control antibody. Each experiment was repeated at least twice, and subsequent raw data files were analyzed with FlowJo software (TreeStar).

Peptide Synthesis using Fmoc/tBU Chemistry

The peptides and their modifications were obtained by solid-phase peptide synthesis using standard Fmoc/tBu chemistry on an Applied Biosystems ABI 433A synthesizer. Removal of protecting groups and cleavage from resin was performed with 2.5% water and 2.5% triisopropylsilane in TFA for 90 min. Deprotected peptides were precipitated in cold diethyl ether. Disulfide bridge formation was performed by adding dissolved peptides (1 mg/mL) in 80% acetic acid/water to the same volume of a 0.25 mg/ml solution of iodine in acetic acid. The reaction was quenched with 20% aqueous ascorbic acid solution after 5 min. Solvents were evaporated and the residue dissolved in 50% acetonitrile in water prior to HPLC-purification (Waters XBridgeBEH130 PREP C18 column 5 µm, 19 × 150 mm). Analyses were performed on an Agilent 1100 HPLC system using a Chromolith Performance RP-C18e column 100 × 3 mm, Merck). 0.1% TFA in water (eluent A) and 0.1% TFA in acetonitrile (eluent B) were used as eluents. Conditions: linear gradient from 0% to 100% B within 5 min with a flow rate of 2 mL/min; UV absorbance λ = 214 nm. The identity of the peptides was verified by HPLC-MS analysis on an Agilent 1200 HPLC system equipped with a Hypersil Gold™ aq-(200 x 2.1 mm)-column (Waters) coupled to an Exactive Orbitrap mass spectrometer (Thermo Fisher Scientific).

Labeling of Peptides with 125Iodine, 68Ga or 177Lutetium

Radiolabeling with ^{125}I was conducted at the tyrosine moiety of the peptides which has been introduced in the SFTI backbone during the library construction (*12*). Labeling was performed by the chloramine-T method (Bailey, G. (2002) The chloramine T Method for Radiolabeling protein, in Protein Protocols Handbook (Walker, J., Ed) pp 963-965, Humana Press). Radiolabeled peptides were purified by analytical HPLC using a Chromolith Performance RP-18e-column, 100 × 4.6 mm (Merck). For DOTA-modifications the peptidyl resin was incubated with 2 equivalents of DOTA p-nitrophenyl-ester and 10 equivalents DIPEA in NMP for 2-16 hrs.

^{68}Ga was eluted with 0.6 M aqueous HCl from a $^{68}Ge/^{68}Ga$ generator (IDB Holland). 1 µL of a 1 mM solution of the respective peptide in 75 µL aqueous 2.5 M sodium acetate, 1 µL saturated ascorbic acid, and 250 ml of ^{68}Ga-generator eluate was heated at 95°C for 10 min at pH 3.6. Purification was performed with a Sola HRP 10 mg SPE cartridge (Thermo). Radiolabeled peptides were eluted with 50% aqueous ethanol. Solvents were evaporated and residual peptides dissolved in appropriate buffer.

5-25 MBq ^{177}Lu chloride (ITG Isotope Technologies, Garching) in 100 ml 0.1 M sodium acetate buffer pH 5 was added to 1 mL of a 1 mM peptide solution. The reaction mixture was heated at 90°C for 15 min and used directly for cell based experiments. The reaction mixture was diluted with 0.9% NaCl (Braun) for animal studies or purified by solid phase extraction for serum stability assays.

Serum Stability Assay

15.7 MBq of the purified ^{177}Lu-radiolabeled peptide was incubated in 200 mL human serum (Sigma-Aldrich) at 37°C. After different time intervals (10 min, 60 min 120 min, 240 min, 24 hours) 10 mL of serum was precipitated with 20 mL acetonitrile. The stability of the labeled peptide was monitored by radio-high pressure liquid chromatography of the supernatant (gradient: 0% to 40% B in 10 min; flow rate: 2 mL/mL; chromolith performance RP18ec (3 mm x

100 mm, Merck). For the detection of radioactive compounds the Agilent 1100 system was equipped with a gamma detector (Packard COBRA™ Auto-Gamma, GMI).

SUPPLEMENTAL FIGURE LEGENDS

SUPPLEMENTAL TABLE 1: Amino acid sequences of SFITGv6 and the natural αvβ6 integrin-specific ligands grafted into the binding loop of the SFTI-1 scaffold. αvβ6 integrin-specific binding motives are in bold.

Peptide name	Binding sequence	Gene symbol	Protein name	AS length	NCBI reference sequence	m/z calculated $[M+2H]^{2+}$	m/z determined $[M+2H]^{2+}$	Retention time [min]	Peptide sequence
SFIFN1	G**RGD**SPAS	FN1	Fibronectin	2386	AAI43755.1	819.8410	819.8124	7.78	GRCTG**RGD**SPASCYPD
SFTNC	R**RGD**MSSN	TNC	Tenascin C	2201	NP_002151.2	907.8776	907.8453	5.23	GRCTR**RGD**MSSNCYPD
SFVTN	T**RGD**VFTM	VTN	Vitronectin	478	NP_000629.3	917.8896	917.8809	10.66	GRCTT**RGD**VFTMCYPD
SFLAP1	R**RGDL**AFI	TGFB1	Transforming growth factor β1	390	NP_000651.3	897.4303	897.3944	8.55	GRCTR**RGDL**AFICYPD
SFLAP3	G**RGDL**GRL	TGFB3	Transforming growth factor β3	412	NP_001316868.1	868.4094	868.3787	9.04	GRCTG**RGDL**GRLCYPD
SFITGv6	F**RGDL**MQL	N/A	N/A	N/A	N/A	936.4211	936.3886	10.58	GRCTF**RGDL**MQLCYPD

SUPPLEMENTAL TABLE 2: Tumor-to-Tissue Ratio of ^{177}Lu-DOTA-SFLAP3 in (A) HNO97 xenografts, (B) HNO399 xenografts, (C) HNO223 xenografts, and (D) ^{177}Lu-DOTA-SFITGv6 in HNO97 xenografts.

Supplemental Table 2A

Tumor-to-Tissue	30 min	60 min	120 min	240 min	360 min
Tumor-to-Blood	5.64±2.86	23.42±12.4	104.48±46.69	296.35±27.2	482.79±201.51
Tumor-to-Heart	14.00±9.04	44.74±9.7	92.17±17.34	124.52±21.91	118.57±32.97
Tumor-to-Lung	3.57±1.63	7.92±0.83	19.92±3.01	21.02±5.64	28.47±7.44
Tumor-to-Spleen	20.71±10.2	62.70±25.09	104.92±17.3	107.93±6.05	94.87±39.27
Tumor-to-Liver	19.30±8.89	42.84±12.74	68.88±11.38	68.12±6.45	53.82±16.65
Tumor-to-Kidney	0.56±0.26	0.94±0.05	1.02±0.2	0.80±0.15	0.76±0.2
Tumor-to-Muscle	15.72±7.72	34.83±6.16	55.90±10.06	73.70±13.73	74.81±16.16
Tumor-to-Intestine	5.16±1.7	8.77±1.6	11.38±2.91	16.42±1.0	14.07±1.94
Tumor-to-Brain	1178.69±750.21	741.00±649.95	847.17±347.64	1073.32±773.31	434.58±88.93

Supplemental Table 2B

Tumor-to-Tissue	30 min	60 min	120 min	240 min	360 min
Tumor-to-Blood	3.03±1.38	8.85±3.63	18.08±7.13	35.07±1.71	51.82±14.03
Tumor-to-Heart	5.23±2.2	10.37±5.11	14.23±4.66	21.45±3.49	19.39±4.31
Tumor-to-Lung	1.15±0.25	1.98±0.56	2.69±0.53	4.07±1.43	3.18±0.83
Tumor-to-Spleen	11.38±6.26	24.60±14.58	20.20±3.25	38.59±14.18	30.22±12.07
Tumor-to-Liver	7.78±3.05	17.07±6.04	18.27±4.97	18.41±5.5	16.39±3.38
Tumor-to-Kidney	0.24±0.12	0.33±0.12	0.24±0.1	0.24±0.07	0.23±0.04
Tumor-to-Muscle	4.85±1.4	9.14±3.21	8.90±5.21	11.66±1.9	13.02±2.81
Tumor-to-Intestine	1.30±0.31	2.54±0.62	2.58±0.62	2.77±0.24	2.46±1.16
Tumor-to-Brain	36.63±20.61	55.18±36.86	40.89±18.02	73.90±11.91	53.27±15.39

Supplemental Table 2C

Tumor-to-Tissue	30 min	60 min	120 min	240 min	360 min
Tumor-to-Blood	2.12±1.63	8.90±2.94	17.14±2.72	57.37±6.23	86.29±58.57
Tumor-to-Heart	3.89±2.89	11.73±2.24	12.18±1.5	20.38±6.12	21.57±3.1
Tumor-to-Lung	0.67±0.5	1.47±0.34	1.48±0.22	2.80±0.45	2.45±0.52
Tumor-to-Spleen	8.08±6.35	24.97±2.93	19.61±3.94	30.68±6.15	27.27±5.81
Tumor-to-Liver	7.03±5.45	20.04±5.3	13.74±1.18	19.66±2.68	19.42±3.55
Tumor-to-Kidney	0.19±0.15	0.31±0.03	0.17±0.02	0.18±0.02	0.18±0.01
Tumor-to-Muscle	3.57±2.6	6.48±2.57	6.82±2.69	13.50±2.99	11.20±5.16
Tumor-to-Intestine	1.02±0.48	1.95±0.68	1.40±0.68	1.89±0.45	1.85±0.42
Tumor-to-Brain	22.41±17.84	63.34±9.4	27.87±23.77	64.03±20.36	58.79±16.48

Supplemental Table 2D

Tumor-to-Tissue	30 min	60 min	120 min	240 min	360 min
Tumor-to-Blood	6.90±0.95	11.72±1.39	41.37±6.25	55.49±15.4	72.00±19.93
Tumor-to-Heart	15.76±1.35	20.34±1.48	41.26±6.21	30.74±11.79	35.69±4.69
Tumor-to-Lung	2.65±0.31	3.37±0.81	5.31±1.57	4.11±1.67	5.85±1.68
Tumor-to-Spleen	19.30±1.54	21.24±2.27	22.93±5.17	12.67±4.36	14.75±2.44
Tumor-to-Liver	16.89±1.02	17.28±2.04	20.10±5.17	9.09±2.74	10.09±1.6
Tumor-to-Kidney	0.15±0.03	0.11±0.03	0.09±0.02	0.04±0.01	0.04±0
Tumor-to-Muscle	16.66±0.27	17.07±1.01	18.77±8.8	10.21±5.65	5.77±3.72
Tumor-to-Intestine	4.68±0.4	5.02±2.24	7.84±2.25	4.90±2.43	5.58±0.76
Tumor-to-Brain	128.71±44.46	150.60±17.54	129.21±79.45	121.31±65.5	122.58±71.73

SUPPLEMENTAL TABLE 3: Maximum Standardized Uptake Values (SUVmax) for PET/CT with ^{68}Ga-DOTA-SFLAP3 for one HNSCC patient.

Tissue/Organ	SUVmax	
	60 min	180 min
Tumor	5.07	4.64
Hilar lymph nodes	4.07	4.15
Plexus choroideus	1.06	1.57
Cerebral parietal	0.05	0.27
Thyroid	3.27	3.24
Blood pool (mediast.)	0.99	1.05
Lung (left)	0.36	0.46
Lung (right)	0.33	0.33
Liver (left)	0.67	0.76
Liver (right)	0.73	0.75
Spleen	0.54	0.8
Pancreas head	2.3	2.62
Stomach	12.65	13.4
Duodenum	6.31	8.91
Jejunum	10.46	9.2
Ileum	4.07	17.65
Kidney (left)	60.52	36.85
Right kidney	22.43	26.41
Colon ascendens	9.2	19.37
Colon descendens	3.75	2.97
Os ileum	0.53	0.47
Muscle (glut.)	1.94	1.92

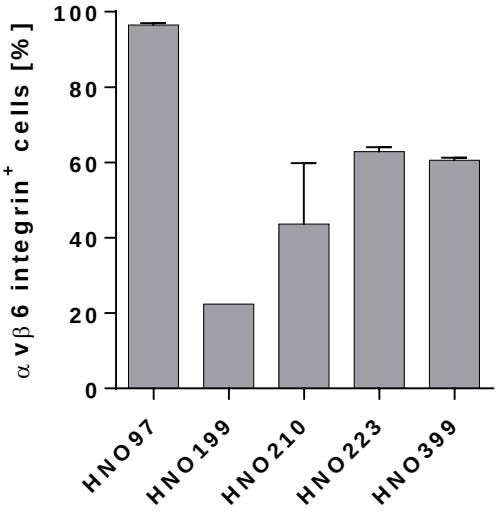

SUPPLEMENTAL FIGURE 1. Flow cytometry of αvβ6 integrin expression in the HNSCC cell lines HNO97, HNO399, HNO199, HNO210, HNO223. Bar graphs represent percentage of αvβ6 integrin-positive cells of three independent biological replicates and standard deviation.

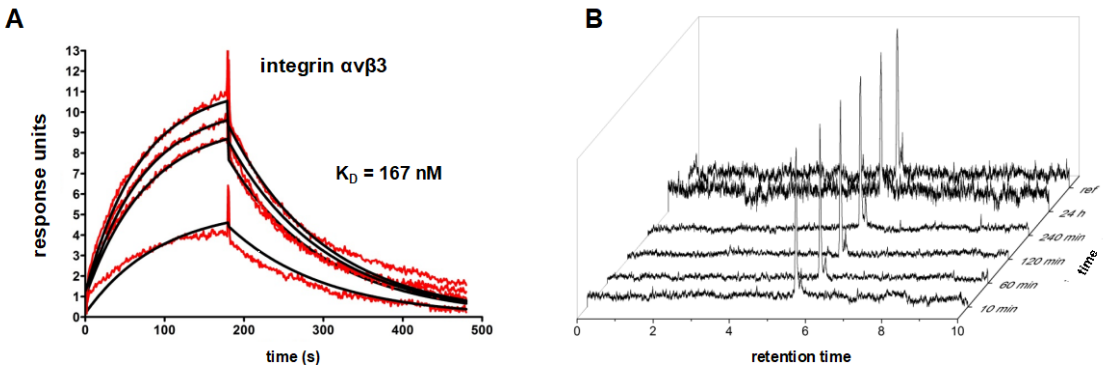

SUPPLEMENTAL FIGURE 2. (A) Affinity of αvβ3 integrin (applied concentrations: 15, 30, 35 and 40 µg/mL) for immobilized SFLAP3 (loading level: 18 response units) was measured by SPR assay (n = 3) with a flow rate of 30 mL/min. The SPR-sensograms were evaluated with the BiaCore evaluation software (black curves) and correspond to the experimentally fitted red curves. K_D values were determined by a 1:1 langmuir model fit of the SPR-sensograms. (B) The stability of ^{177}Lu-DOTA-SFLAP3 in human serum was evaluated by radio-high pressure liquid chromatography after 10, 60, 120, 240 min and 24 hrs.

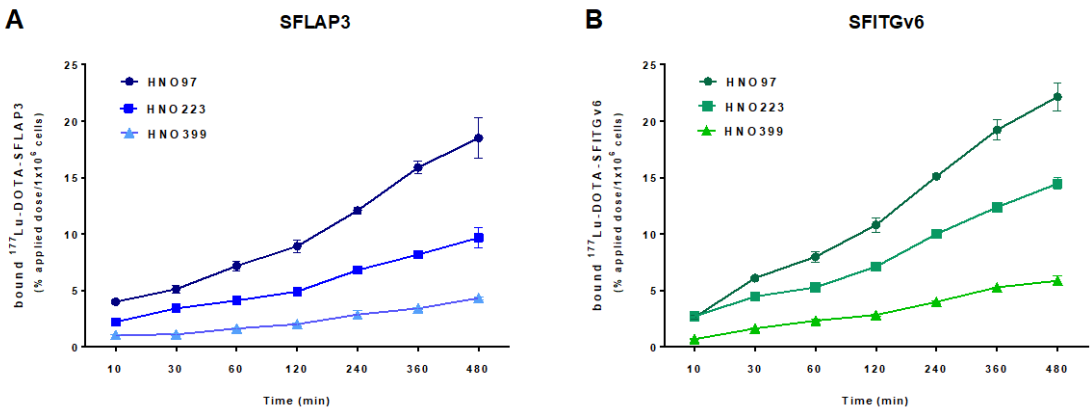

SUPPLEMENTAL FIGURE 3. Binding of ^{177}Lu-DOTA-labeled SFLAP3 (A) and SFITGv6 (B) to HNO97, HNO399, and HNO223 cells after incubation for 10, 30, 60, 120, 360, and 480 min, respectively. The amount of bound peptide (percentage of applied dose per 10^6 HNSCC cells) increased over time. Data represent mean values and standard deviation of triplicate measurements from representative experiment.

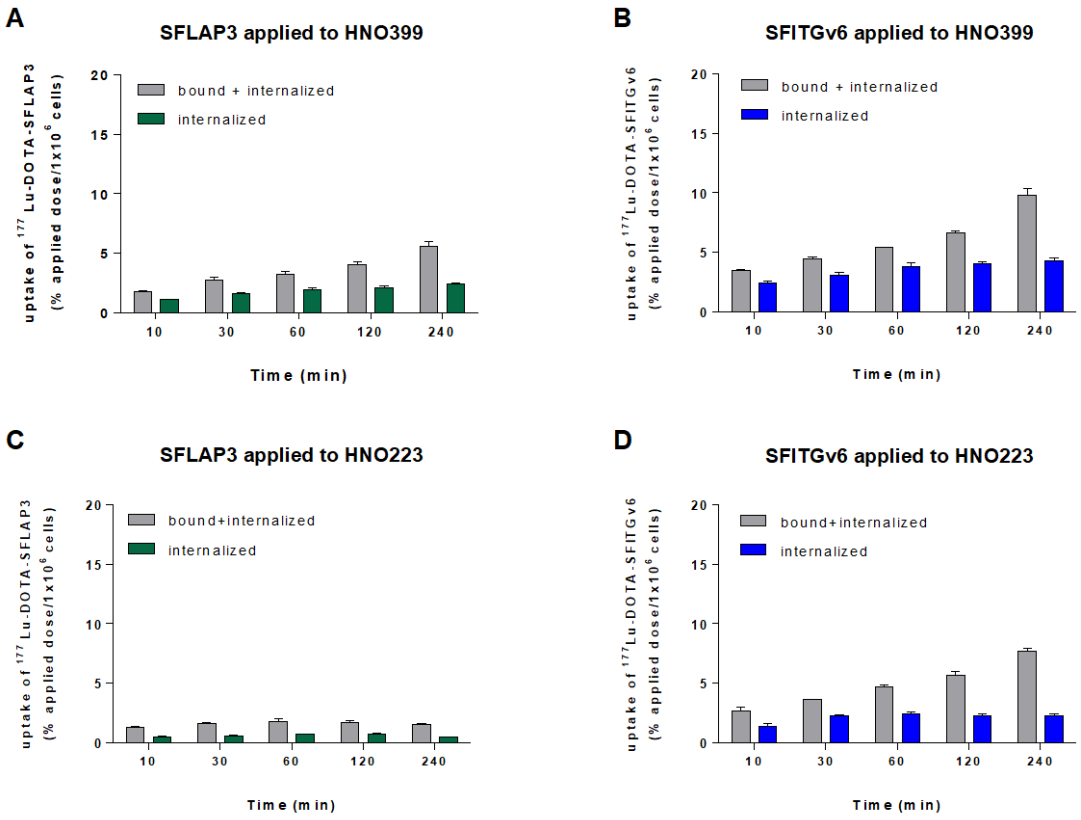

SUPPLEMENTAL FIGURE 4. Uptake (grey bars) and internalization (colored bars) of ^{177}Lu-DOTA-labeled SFLAP3 (A and C) and SFITGv6 (B and D) in HNO399 (A and B) and HNO223 cells (C and D). After incubation for 10, 30, 60, 120, and 240 min, respectively, the radioactivity in the lysates was determined and calculated as % applied dose/10^6 cells. Data represent mean values and standard deviation of triplicate measurements from representative experiment.

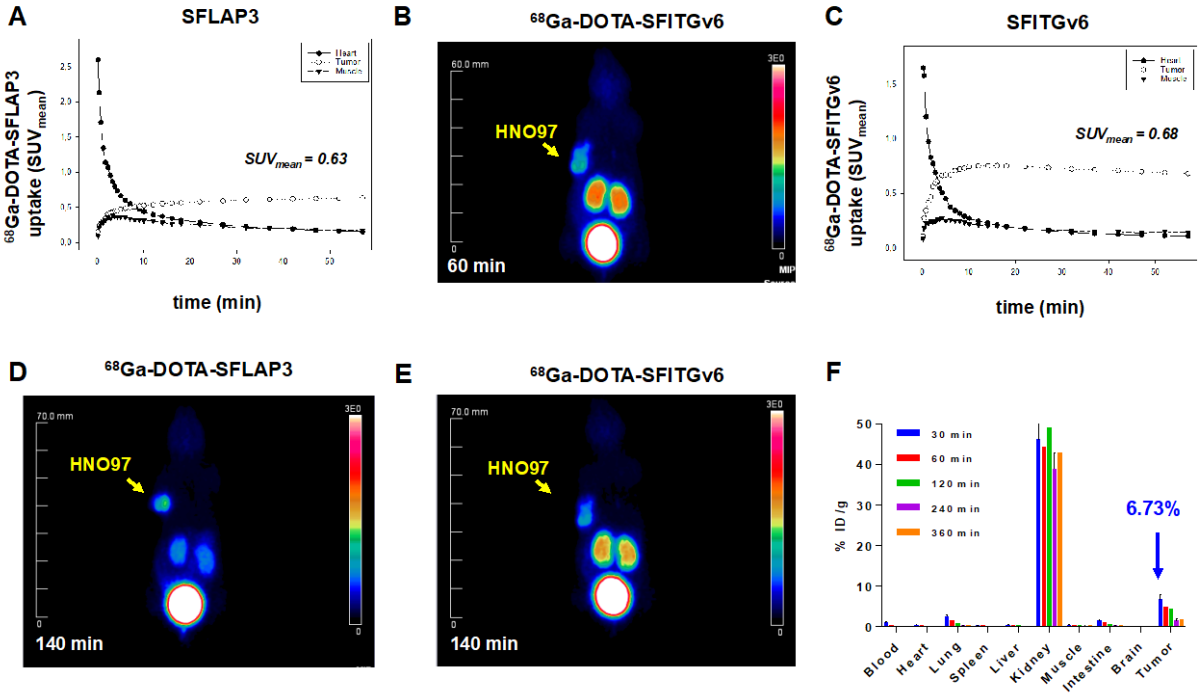

SUPPLEMENTAL FIGURE 5. (D) Small-animal PET imaging of HNO97 xenograft mouse 140 min after injection of ^{68}Ga-DOTA-SFLAP3 (37.9 MBq) and (A) time activity curve (SUVmean) up to 60 min. (C) Time activity curve (SUVmean) up to 60 min and small-animal PET imaging of HNO97 xenograft mouse (B) 60 min and (E) 140 min after injection of ^{68}Ga-DOTA-SFITGv6 (30 MBq). (F) Biodistribution of ^{177}Lu-DOTA-SFITGv6 (% ID/g) in tumors and organs of HNO97 xenograft mice (n=3) measured 30, 60, 120, 240, and 360 min after injection of 1 nmol (1 MBq) peptide. Data are shown as mean of three per time point and standard deviation.

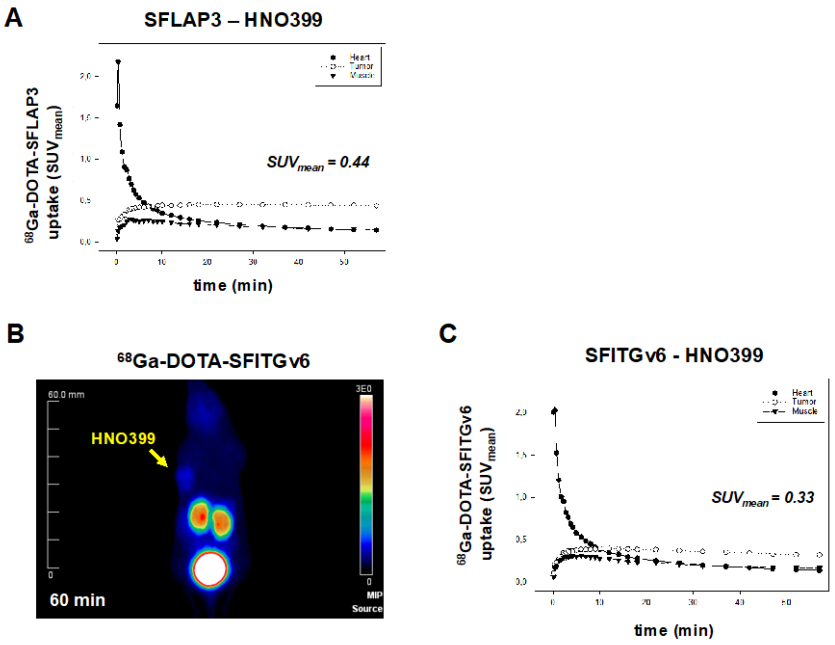

SUPPLEMENTAL FIGURE 6. (A) Time activity curve (SUVmean) calculated for small-animal PET imaging of HNO399 xenograft mouse after injection of ^{68}Ga-DOTA-SFLAP3 (26 MBq). (B) Small-animal PET imaging and (C) time activity curve (SUVmean) of a HNO399 xenograft mouse 60 min after injection of ^{68}Ga-DOTA-SFITGv6 (34 MBq).

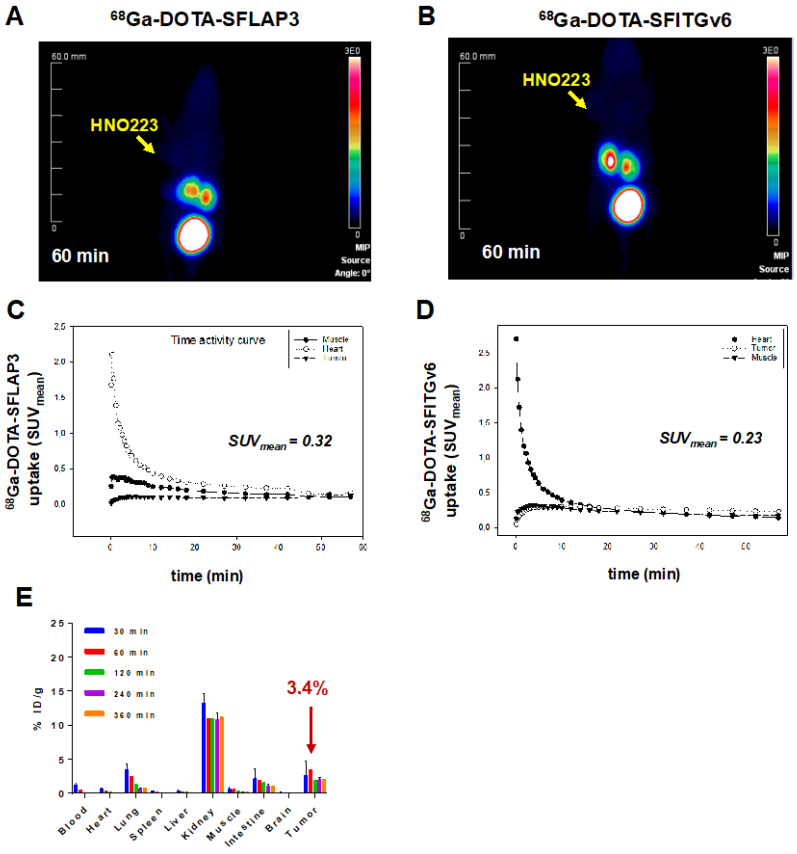

SUPPLEMENTAL FIGURE 7. (A and B) Small animal PET imaging and (C and D) time activity curves (SUVmean) of HNO223 xenograft mice 60 min after injection of (A and C) ^{68}Ga-DOTA-SFLAP3 (27 MBq) and (B and D) ^{68}Ga-DOTA-SFITGv6 (34 MBq). (E) Biodistribution of radioactivity (% ID/g) in tumors and organs of HNO223 xenograft mice (n=3) measured 30, 60, 120, 240, and 360 min after injection of 1 nmol (1 MBq) ^{177}Lu-DOTA-SFLAP3. Data are shown as mean of three per time point and standard deviation.